Absolute cross sections for electron-impact single ionization of Ne^{q+} ($q=2,4-6$) ions

M. E. Bannister

Physics Division, Oak Ridge National Laboratory, Oak Ridge, Tennessee 38731-6372

Absolute total cross sections for electron-impact single ionization of Ne^{q+} ($q=2,4-6$) ions have been measured using a crossed-beams technique from below the ground-state ionization threshold to 800 eV with typical total uncertainties near the peak of the cross sections ranging from 9% for Ne^{2+} to 13% for Ne^{6+}. Details of the apparatus and experimental procedures used in this study are presented along with a discussion of the experimental uncertainties. The measured cross sections for all four ions are dominated by direct ionization and are in excellent agreement with the Lotz semiempirical formula. Ionization rate coefficients and fitting parameters calculated from the measured cross sections are also reported. [S1050-2947(96)03008-9]

I. INTRODUCTION

The need for atomic data to support fusion research has resulted in a wealth of cross sections for electron-impact ionization of ions [1]. Surprisingly, there have been few reports of absolute electron-impact ionization cross section measurements for multicharged neon ions. Experimental cross sections for only Ne^{2+}, [2,3] Ne^{3+}, [4], and Ne^{7+} [5] have been published. Ionization cross sections for neon are critical in modeling and diagnosing the ITER tokamak since neon is a prime candidate impurity for radiation power exhaustion in the divertor [6]. Neon has higher radiation emission rates than lower-Z species such as Be and C, and a higher impurity fraction of Ne can exist in an ignited plasma than of higher-Z impurities such as Ar. This paper presents absolute total cross sections for electron-impact ionization of Ne^{q+} for $q=2,4,5,6$.

The ionization cross sections reported here were measured using the Oak Ridge National Laboratory (ORNL) electron-ion crossed-beams apparatus. The experimental results are compared to previous measurements and calculations where available. Comparisons to the Lotz [7] semiempirical formula and to data recommended by Lennon *et al.* [8] are also made.

II. EXPERIMENT

The experimental method and ORNL crossed-beams apparatus have been described in detail elsewhere [9], but numerous changes since that time make an updated description necessary. A schematic drawing of the apparatus is shown in Fig. 1. The production, transport, and measurement of the incident ion and electron beams will be discussed in the first section below. The next sections will detail the procedures used for measuring absolute cross sections and the associated experimental uncertainties.

A. Ion and electron beams

Neon ions are extracted from the ORNL electron-cyclotron-resonance (ECR) ion source at 10 kV and mass analyzed by a 90° bending magnet. The ion source is typically operated with 20–50 W of microwave power and a gas

pressure of about 10^{-4} Pa (10^{-6} Torr) in the ECR region. For these experiments, both ^{20}Ne and ^{22}Ne isotopes were used in order to eliminate possible errors due to impurity ions with the same mass-to-charge ratios. Cross sections measured with the two isotopes were indistinguishable within the experimental uncertainties, indicating that ion beam impurities were negligible. The ion beam is charge-purified by an electrostatic parallel-plate analyzer just upstream of the collision volume (see Fig. 1). This eliminates any ions that have undergone charge exchange in the several-meter beamline between the mass analyzing magnet and the charge purifier. The ions enter the magnetically shielded collision volume through a 0.5 cm wide by 1.0 cm high aperture and are crossed perpendicularly by the electron beam. Upon exiting the collision volume through another 0.5 cm by 1.0 cm aperture, the product $Ne^{(q+1)+}$ ions are separated from the primary Ne^{q+} ion beam by a double-focusing magnet. The product ions are magnetically deflected horizontally through 90° and then are deflected vertically 90° out of the plane of the magnetic dispersion by an electrostatic curved-plate analyzer and onto a channel electron multiplier. This analyzer (vertical deflector) is shown in the plane of Fig. 1 for ease of presentation only. The position of the product ions in the detector plane can be adjusted in two dimensions
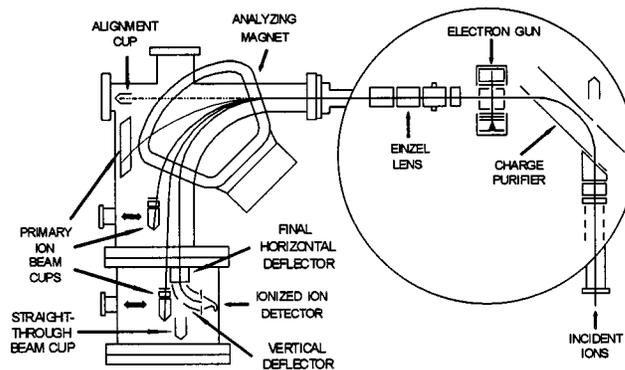

FIG. 1. Electron-ion crossed-beams experimental apparatus. See text for an explanation.

using the curved-plate analyzer and a final horizontal deflector located between the magnet and the analyzer.

The primary neon ions are collected by one of three Faraday cups (two are movable) shown in Fig. 1. The charge ratio of the primary and product ions determines which cup is used and its position. For the Ne^{2+} measurements, the first (fixed) Faraday cup was used; for the other measurements, the middle Faraday cup was used. The Ne^{2+} ion current measurements were corrected to account for incomplete ion current collection and lack of secondary electron suppression by the fixed Faraday cup. The ratio of true ion current (as measured in the middle Faraday cup with secondary electron suppression) to the current measured in the fixed cup ranged from 1.06 to 1.19 in the present experiments. Typical ion beam currents ranged $100-250$ nA for ^{22}Ne^{q+} and $0.9-1.5$ μA for ^{20}Ne^{q+}.

The electron beam is generated as follows. An immersion lens draws electrons from an indirectly heated cathode into a focus and a cylinder-aperture (rectangular geometry) lens makes the beam parallel [10]. The gun, collision volume, and collector are magnetically shielded to reduce fields in these regions to less than 40 mG. After passing through the collision volume, the electrons are driven by a transverse electric field onto a collector plate covered with metal ''honeycomb.'' The electron current to the box surrounding the collision volume is less than 1% of the total collector electron current. For electron energies less than 150 eV, a fraction of the electron current passing through the collision volume strikes a grounded shielding electrode between the collision volume and the collector. The measured electron current is taken to be the sum of the currents to the collector and the shield since beam profile measurements demonstrate that some of the electrons striking this shield pass through the ion beam. The electron beam is chopped at 1 kHz during data acquisition by applying a 50%-duty-cycle square-wave voltage to the extraction electrode of the gun.

The differential distributions (profiles) of the electron and ion beams in the direction perpendicular to both beams (that is, in the vertical direction), denoted by $I_e(z)$ and $I_i(z)$, respectively, are measured using a stepping-motor-driven L-shaped beam probe with coplanar slits, each 0.15 mm wide. Typical beam profiles are shown in Fig. 2. Combinations of these current profiles are integrated numerically to obtain the ''form factor'' F, the geometric term quantifying the overlap of the two beams [10], calculated by

$$F = \frac{\int I_e(z)dz \int I_i(z)dz}{\int I_e(z)I_i(z)dz}. \quad (1)$$

B. Diagnostics

Elimination of any spurious sources of apparent signal is crucial for accurately determining absolute ionization cross sections. Since the background detector counts arise predominantly due to the ion beam, with a small contribution from detector dark counts, ion beam tuning is critical. The two major sources of spurious signal in this experiment both result from modulation of the ion background by the chopped electron beam. The first, pressure modulation, can occur because the intense electron beam causes an increase in the background gas pressure in the collision volume, thus
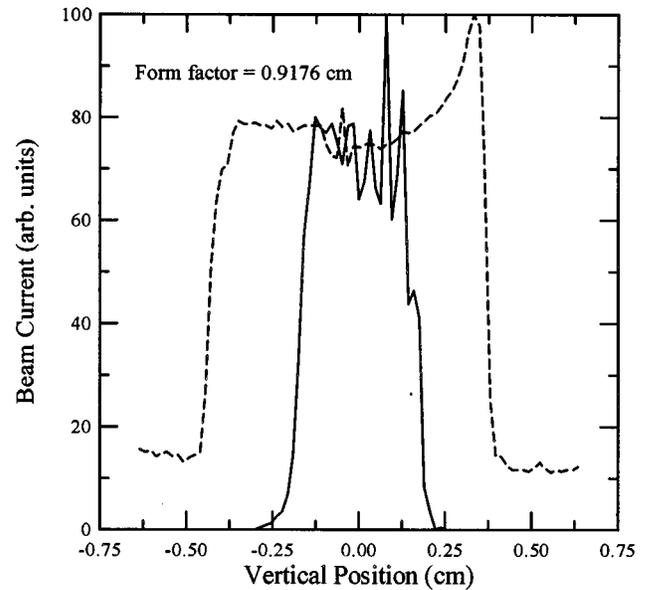

FIG. 2. Typical ion and electron beam profiles in the interaction region along the direction perpendicular to both beams. The solid curve is a 60 keV Ne^{6+} ion beam; the dashed curve 500 eV electrons.

increasing the number of ions stripped on the background gas. This effect is eliminated by using a sufficiently high chopping frequency, in this case 1 kHz, in order that the pressure does not vary over one chop period. In addition, the electron gun is left on overnight at a few hundred eV to keep the surfaces in the gun and collector degassed. The electron collector is also heated continuously by current-carrying nichrome wires located below the collector plate and honeycomb. The second source of spurious signal is modulation of ion background resulting from a small fraction of the primary ion beam striking a ground shield in front of the Faraday cup. Proper tuning of the ion optics upstream of the collision volume reduces the ion current to this shield to less than 0.1 nA so that any apparent signal produced is negligible compared to the real ionization signal.

After the ion optics upstream of the collision box are optimized for maximum current and minimum background, the downstream optics are adjusted to assure full collection of the product ions. The analyzer magnet is set approximately by steering the primary ion beam into the straight-through Faraday cup (see Fig. 1) with the other downstream optics off and then scaling the magnetic field down by the ratio of the parent-to-product charge ratio so that the product ions are now deflected through 90°. Then the downstream optics are turned on and the signal is measured at a particular electron energy as the magnetic field is varied in small steps. A typical resulting scan is shown in Fig. 3(a) for ionization of Ne^{6+} at an electron energy of 500 eV. The magnetic field is chosen in the middle of the flat peak of the scan. Once the optimum magnetic field is determined, the voltage on the curved-plate analyzer is varied with the other downstream optics held constant. Figure 3(b) shows a typical scan over the curved-plate analyzer voltage. Next, the optimum voltage for the final horizontal deflector is determined, as illustrated by the example in Fig. 3(c). The flat peaks on the three
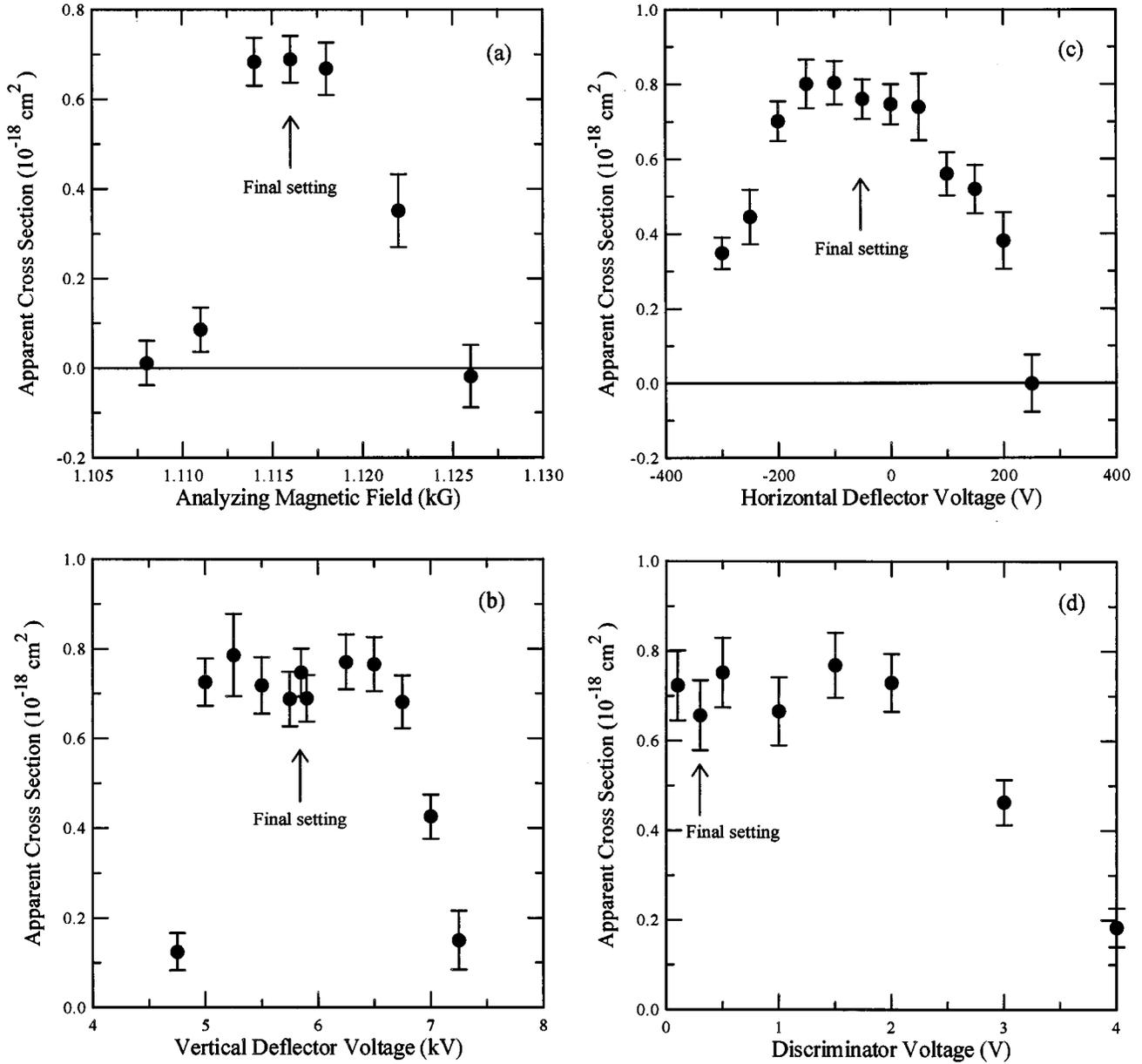
FIG. 3. Typical diagnostic scans with apparent cross section plotted versus experimental parameters for Ne^{6+} at an electron energy of 500 eV: (a) analyzing magnetic field, (b) vertical deflector voltage, (c) horizontal deflector voltage, and (d) pulse discriminator lower-limit voltage.

downstream optics scans indicate that full collection of the product ions has been achieved.

The final diagnostic performed is the measurement of the signal pulse transmission through the detector electronics. With 2.8 kV applied to the channeltron and an amplifier gain of 50, the pulse height distribution (PHD) is measured by varying the lower limit of a ''voltage-window'' discriminator in small steps and measuring the net signal. A typical result is shown in Fig. 3(d) for Ne^{6+} ionization at 500 eV. Extrapolation of the net signal to zero discriminator setting determines the true signal; the pulse transmission is the ratio of the signal at the discriminator setting used for the experiment (in this case, 0.3 V) to the true signal. The pulse transmission was estimated to be between 0.98 and 1.00 for the present experiments. No corrections were made to the measured cross sections to account for a nonunity pulse trans-

mission; however, uncertainty in this quantity was included in the absolute uncertainty of the measurements as discussed below.

C. Absolute cross sections and uncertainties

The absolute cross sections are determined [11] from the measurements using

$$\sigma(E) = \frac{R}{I_i I_e} \frac{q e^2 v_i v_e}{\sqrt{v_i^2 + v_e^2}} \frac{F}{D}, \tag{2}$$

where $\sigma(E)$ is the absolute cross section at the center-of-mass electron-impact energy E, R is the product ion count rate, I_i and I_e are the incident ion and electron currents, qe is the charge of the incident ions, v_i and v_e are the incident ion

TABLE I. Absolute uncertainties. All uncertainties are at a high confidence level (equivalent to a 90% confidence level on the statistical uncertainties). These are combined with total relative uncertainties at a 90% confidence level to yield the total uncertainties of the measurements.

Source	Uncertainty (%)
Product ion detection and pulse transmission	± 5
Transmission of product ions to detector	± 4
Absolute value of form factor	± 4
Ion current measurement	± 2
Electron current measurement	± 2
Ion velocity	± 1
Electron velocity	± 1
Quadrature sum	± 8.2

TABLE II. Experimentally measured absolute total cross sections for electron-impact single ionization of Ne^{2+}. The relative uncertainties are at the one-standard-deviation level; the total uncertainties (given in parentheses) are at a high confidence level corresponding to 90% confidence for the relative uncertainties.

E (eV)	σ $(10^{-18}\ cm^2)$
56.0	1.47 ± 0.71 (1.42)
60.9	0.12 ± 0.59 (1.19)
62.9	0.48 ± 0.50 (1.00)
63.9	0.39 ± 0.51 (1.01)
64.9	0.27 ± 0.47 (0.95)
65.9	1.43 ± 0.44 (0.90)
70.9	4.18 ± 0.59 (1.23)
80.9	7.09 ± 0.45 (1.08)
90.9	9.75 ± 0.40 (1.13)
100.8	11.78 ± 0.30 (1.14)
110.8	13.40 ± 0.34 (1.29)
125.7	14.86 ± 0.33 (1.39)
150.6	16.95 ± 0.36 (1.57)
175.4	17.20 ± 0.38 (1.60)
200.3	17.88 ± 0.39 (1.66)
225.4	18.12 ± 0.40 (1.69)
250.4	18.50 ± 0.40 (1.72)
275.4	18.18 ± 0.41 (1.70)
300.4	18.12 ± 0.38 (1.67)
325.5	17.39 ± 0.41 (1.65)
350.6	17.37 ± 0.37 (1.61)
375.7	16.53 ± 0.38 (1.56)
400.6	16.70 ± 0.35 (1.54)
450.6	16.18 ± 0.37 (1.52)
500.6	15.85 ± 0.37 (1.49)
550.7	14.69 ± 0.37 (1.41)
600.8	14.20 ± 0.31 (1.32)
700.9	13.28 ± 0.34 (1.28)
800.9	11.92 ± 0.34 (1.19)

and electron velocities, F is the form factor that is determined from the two beam profiles, and D is the channeltron detection efficiency for the product ions that we estimated to be 98% [4].

The components of the absolute uncertainty for the measurements are given in Table I at a level equivalent to a 90% confidence level for statistical uncertainties. The dominant contributions come from the transmission of product ions to the detector, product ion detection and pulse transmission, and measurement of absolute form factors. A detailed discussion of each of these sources has been given previously [9]. Although some of the values have been recently adjusted, the general discussion in this reference is still valid. The quadrature sum of these components is $\pm 8.2\%$. Combining this sum with the total relative uncertainties at a 90% confidence level (two standard deviations) yields the total uncertainty for the measurements, shown in parentheses in Tables II-V.

The error bars shown in the figures are relative uncertainties only and are displayed at the one-standard-deviation level. The relative uncertainties are the quadrature sum of the statistical uncertainties and a 2% contribution from form factor variations. These relative uncertainties are also given in Tables II-V at the one-standard-deviation level.

III. RESULTS

The experimental results will be discussed in separate sections for each of the charge states. However, some discussion that is common to all four charge states is more conveniently given here. For each of the ions, experimental cross sections will be compared to the one-parameter Lotz semiempirical formula [7], except for Ne^{2+}, where the three-parameter form is used, and to the recommended cross sections given in the compilation of Lennon et al. [8]. Few experimental ionization cross sections have been reported for multicharged neon ions. For Ne^{2+}, researchers at Nagoya have published crossed-beams results [2,3] and Hasted et al. [12,13] trapped ion measurements. Only the electron beam ion source (EBIS) measurements of Donets and Ovsyannikov [14] for energies greater than 3 keV have been reported for ionization of the other three charge states. The present cross sections are also

compared to scaled measurements for isoelectronic multi-charged ions.

Theoretical cross sections are likewise scarce in the literature. Jakubowicz and Moores [15] published distorted-wave calculations for Ne^{6+}. Salop [16] calculated cross sections in the binary-encounter approximation (BEA) for the four ions discussed in this paper, but his results overestimate the peak cross sections by $30-50\%$ and fall off faster with energy than the Born approximation ($\ln E/E$).

A. Ne^{2+}

Measured absolute total cross sections for electron-impact single ionization of Ne^{2+} from 56 eV to 800 eV are shown in Fig. 4 with the threshold region displayed in the inset. The solid circles represent the present measurements and the open triangles the results of Matsumoto et al. [3]. Also presented is a solid line representing the three-parameter Lotz semiempirical formula [7] for direct ionization of the $2s^2 2p^4$ ground state configuration, and a dashed line representing the cross section curve recommended in the compi-

TABLE III. Experimentally measured absolute total cross sections for electron-impact single ionization of Ne^{4+}. The relative uncertainties are at the one-standard-deviation level; the total uncertainties (given in parentheses) are at a high confidence level corresponding to 90% confidence for the relative uncertainties.

E (eV)	σ (10^{-18} cm^2)
110.5	0.14 ± 0.29 (0.58)
115.5	-0.07 ± 0.32 (0.64)
120.8	-0.07 ± 0.17 (0.35)
123.3	0.26 ± 0.19 (0.38)
125.8	0.24 ± 0.16 (0.31)
128.3	0.32 ± 0.20 (0.40)
130.8	0.43 ± 0.13 (0.26)
136.0	1.17 ± 0.28 (0.57)
141.0	1.30 ± 0.17 (0.37)
145.9	1.46 ± 0.32 (0.64)
151.0	1.95 ± 0.20 (0.43)
155.9	1.81 ± 0.22 (0.47)
160.8	2.38 ± 0.14 (0.35)
170.7	2.66 ± 0.21 (0.46)
180.7	2.84 ± 0.18 (0.43)
190.6	3.14 ± 0.19 (0.45)
200.7	3.34 ± 0.09 (0.33)
225.7	3.52 ± 0.17 (0.44)
250.7	3.56 ± 0.17 (0.44)
275.7	3.68 ± 0.16 (0.43)
300.8	3.94 ± 0.14 (0.43)
325.8	3.87 ± 0.14 (0.42)
350.8	4.06 ± 0.13 (0.42)
375.9	3.93 ± 0.15 (0.43)
400.8	4.12 ± 0.12 (0.41)
425.7	4.07 ± 0.14 (0.44)
450.8	4.01 ± 0.14 (0.43)
475.8	4.06 ± 0.12 (0.42)
500.6	3.98 ± 0.11 (0.40)
550.7	3.76 ± 0.11 (0.38)
600.7	3.61 ± 0.15 (0.42)
650.6	3.48 ± 0.16 (0.43)
700.6	3.52 ± 0.14 (0.40)
750.5	3.22 ± 0.13 (0.37)
800.3	2.91 ± 0.10 (0.32)

TABLE IV. Experimentally measured absolute total cross sections for electron-impact single ionization of Ne^{5+}. The relative uncertainties are at the one-standard-deviation level; the total uncertainties (given in parentheses) are at a high confidence level corresponding to 90% confidence for the relative uncertainties.

E (eV)	σ (10^{-18} cm^2)
145.9	0.05 ± 0.09 (0.19)
151.0	-0.02 ± 0.07 (0.13)
156.0	0.01 ± 0.08 (0.15)
158.4	0.03 ± 0.09 (0.19)
160.9	0.17 ± 0.07 (0.14)
166.0	0.27 ± 0.07 (0.14)
171.0	0.46 ± 0.08 (0.16)
175.9	0.63 ± 0.08 (0.18)
201.0	0.87 ± 0.06 (0.14)
225.9	1.11 ± 0.09 (0.20)
250.9	1.49 ± 0.07 (0.18)
275.9	1.66 ± 0.06 (0.19)
301.2	1.69 ± 0.06 (0.18)
326.0	1.65 ± 0.06 (0.18)
351.1	1.76 ± 0.08 (0.21)
376.1	1.84 ± 0.07 (0.21)
401.2	1.80 ± 0.05 (0.17)
426.2	1.78 ± 0.11 (0.26)
451.1	1.79 ± 0.07 (0.21)
476.2	1.67 ± 0.10 (0.24)
501.2	1.74 ± 0.05 (0.18)
551.0	1.73 ± 0.07 (0.20)
601.2	1.71 ± 0.05 (0.17)
651.3	1.59 ± 0.05 (0.17)
701.3	1.55 ± 0.05 (0.16)
751.2	1.60 ± 0.05 (0.16)
801.2	1.47 ± 0.05 (0.15)

The present data are also compared in a Bethe plot (Fig. 5) to results for Si^{6+} reported previously [18]. The scaled experimental cross section times the scaled electron energy is plotted versus the logarithm of the scaled electron energy. This scaling is commonly used for predicting ionization cross sections for a given ion based on existing data for isoelectronic ions. Both curves are almost linear, as indicated by the least-squares fit lines in Fig. 5, but the slope of the Si^{6+} data is about 50% larger than that for the Ne^{2+} data.

B. Ne^{4+}

Figure 6 illustrates the measured cross sections for Ne^{4+} from 120 eV to 800 eV, and again the experimental results are also presented in Table III. The total uncertainty near the peak of the cross section is typically 10%. The solid and dashed curves are the Lotz semiempirical formula for direct ionization of the ground state and the recommended data of Lennon et al. [8] based on scaling of O^{2+} calculations, respectively.

The agreement between the present measurements and the Lotz formula is quite good, differing by only a few percent near the peak and lying well within the total uncertainty. The

lation of Lennon et al. [8] and based on the data of Danjo et al. [2]. The present experimental data are also given in Table II; the total uncertainty near the peak of the cross section is typically 9%.

The present measurements are in reasonable agreement with the results of Matsumoto et al. [3] and with the Lotz semiempirical formula, exceeding both by less than 10% near the peak and being dominated by direct ionization. The only significant difference between the two sets of experimental data is that the present data fall off as $(\ln E/E)$ above 400 eV while the data of Matsumoto et al. decreases more slowly. As shown in the inset of Fig. 4, zero measured cross sections below the ground state ionization threshold [17] of 63.45 eV indicate an absence of metastable ions in the primary Ne^{2+} ion beam.

TABLE V. Experimentally measured absolute total cross sections for electron-impact single ionization of Ne^{6+}. The relative uncertainties are at the one-standard-deviation level; the total uncertainties (given in parentheses) are at a high confidence level corresponding to 90% confidence for the relative uncertainties.

E (eV)	σ $(10^{-18}$ $cm^2)$
181.3	0.009 ± 0.034 (0.068)
201.4	0.016 ± 0.022 (0.044)
206.4	0.067 ± 0.027 (0.054)
211.4	0.098 ± 0.024 (0.049)
216.4	0.125 ± 0.025 (0.051)
226.4	0.246 ± 0.031 (0.066)
251.3	0.309 ± 0.039 (0.083)
276.3	0.466 ± 0.035 (0.080)
301.5	0.605 ± 0.028 (0.074)
326.6	0.670 ± 0.040 (0.098)
351.6	0.696 ± 0.028 (0.080)
376.7	0.721 ± 0.031 (0.086)
401.7	0.715 ± 0.019 (0.070)
451.6	0.664 ± 0.026 (0.075)
501.6	0.693 ± 0.023 (0.073)
551.6	0.723 ± 0.024 (0.076)
601.6	0.715 ± 0.025 (0.077)
651.6	0.688 ± 0.025 (0.076)
701.6	0.678 ± 0.024 (0.074)
751.6	0.679 ± 0.023 (0.072)
801.5	0.667 ± 0.027 (0.076)
901.3	0.665 ± 0.027 (0.076)
1001.4	0.660 ± 0.024 (0.072)

FIG. 4. Absolute cross sections as a function of electron-impact energy for single ionization of Ne^{2+}. The present experimental results are indicated by the solid circles with relative uncertainties at the one-standard-deviation level. The open triangles are the measurements of Ref. [3]. The solid curve is the prediction of the three-parameter Lotz formula and the dashed curve represents the cross sections recommended in Ref. [8]. The inset shows the threshold region with a linear energy scale; the results of Ref. [3] are omitted for clarity.

curve recommended by Lennon *et al.* underestimates the cross section by 10–15% near the peak, but agrees well with the measurements near threshold, as shown in the inset of Fig. 6. The small cross sections measured below the ground state threshold [17] of 126.21 eV suggest that a few percent of the Ne^{4+} ion beam could have been in a metastable state, but the statistical uncertainties of these points make a reasonable estimate of the metastable fraction impractical.

The Bethe plot of Fig. 7 compares the present results with scaled cross sections from prior measurements on O^{2+} [19]. The curves are almost identical, with the Ne^{4+} data just a few percent higher over most of the energy range of the measurements. This is one case where scaling of the ionization cross sections yields very good agreement between the data.

C. Ne^{5+}

The measured cross sections for ionization of Ne^{5+} from 150 eV to 800 eV are shown in Fig. 8 and also given in Table IV. The solid curve represents the Lotz formula and the dashed curve is recommended by Lennon *et al.* [8] based on scaling calculations for O^{3+}. The total uncertainty for the present data is typically 11% near the peak of the cross section.

The measurements agree very well with the Lotz prediction over most of the energy range except near threshold (see the inset of Fig. 8) where the experimental results are some-
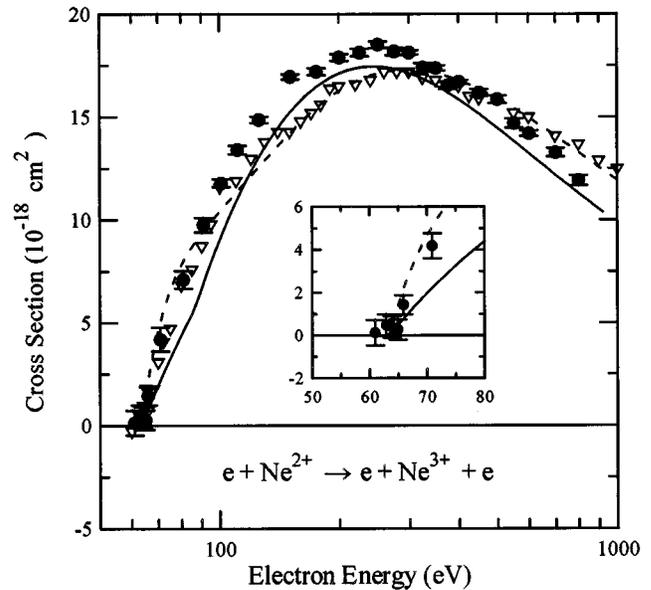
what higher. The peak cross section is identical to the Lotz formula and only a few percent higher than the recommended curve of Lennon *et al.* The zero cross section below the ground state threshold [17] of 157.93 eV indicates the
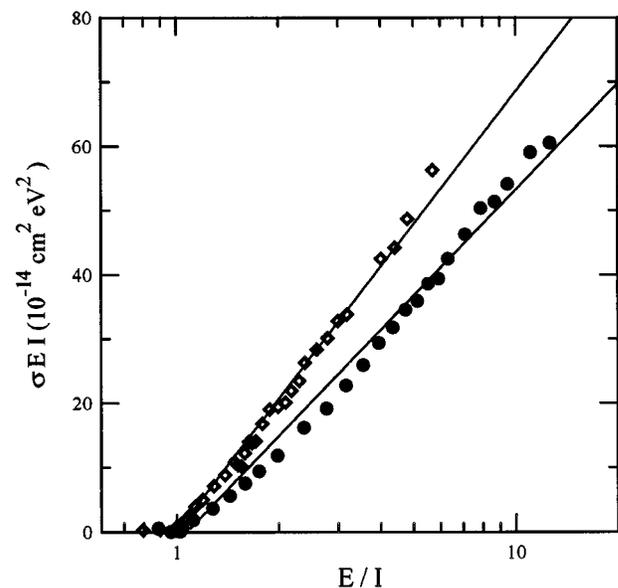

FIG. 5. Bethe plot of product of scaled electron impact ionization cross sections times reduced energy versus the logarithm of the reduced energy for O-like ions. The circles are the present results for Ne^{2+} and the diamonds are measurements for Si^{6+} from Ref. [17]. The lines are least-squares fits to the experimental points.
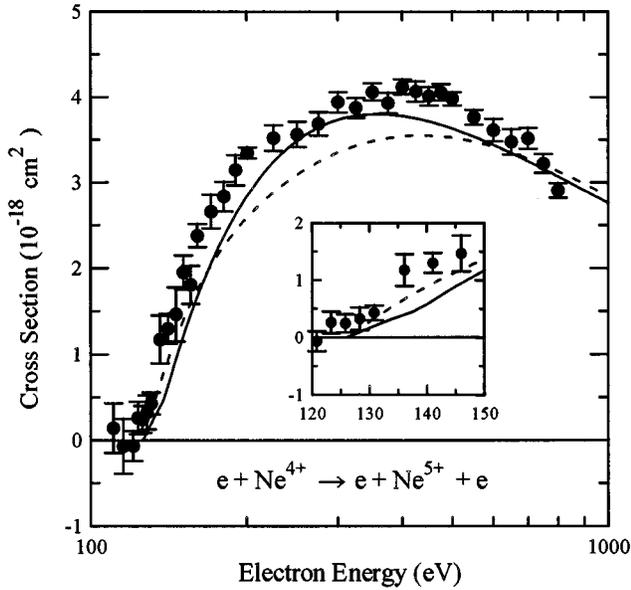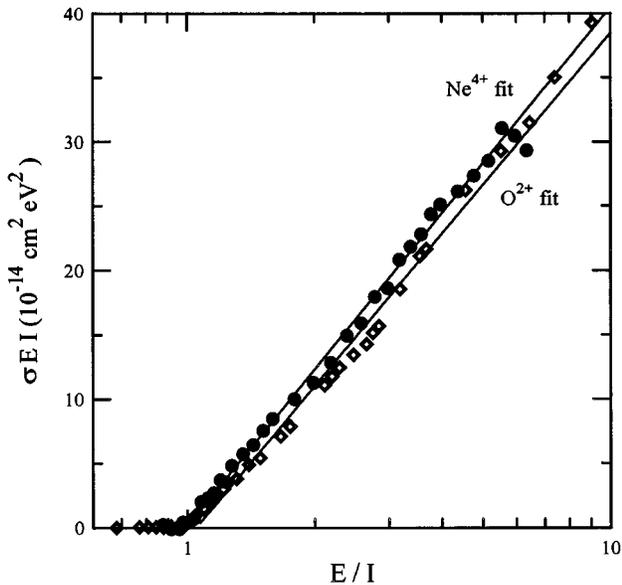
FIG. 6. Absolute cross sections as a function of electron-impact energy for single ionization of Ne^{4+}. The present experimental results are indicated by the solid circles with relative uncertainties at the one-standard-deviation level. The solid curve is the prediction of the one-parameter Lotz formula and the dashed curve represents the cross sections recommended in Ref. [8]. The inset shows the threshold region with a linear energy scale.
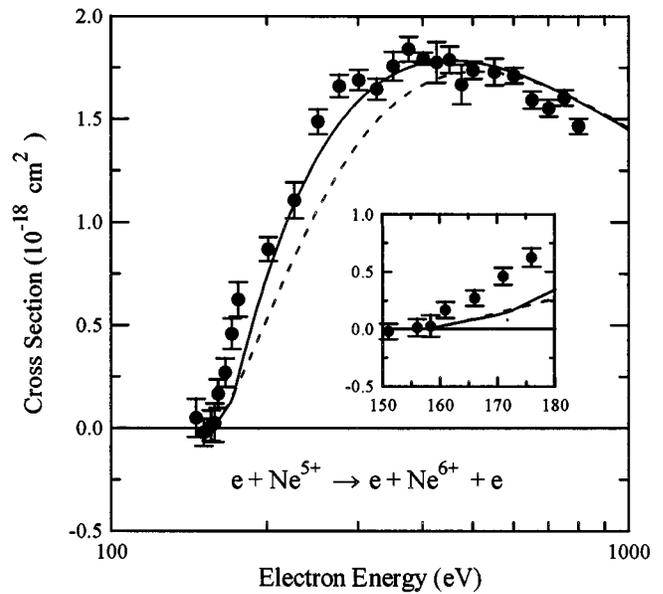

FIG. 8. Absolute cross sections as a function of electron-impact energy for single ionization of Ne^{5+}. The present experimental results are indicated by the solid circles with relative uncertainties at the one-standard-deviation level. The solid curve is the prediction of the one-parameter Lotz formula and the dashed curve represents the cross sections recommended in Ref. [8]. The inset shows the threshold region with a linear energy scale.

absence of metastable ions in the Ne^{5+} beam.

Figure 9 shows a Bethe plot of the present data along with measurements for ionization of N^{2+} [20] and O^{3+} [21]. The scaling is excellent over the range of the neon measurements as the three curves are nearly indistinguishable. It is interest-

ing to note that although no metastables were apparent in the N^{2+} and Ne^{5+} ion beams extracted from the ORNL ECR ion source, a metastable fraction of about 16% was estimated for the O^{3+} ion beam extracted from the old ORNL Penning
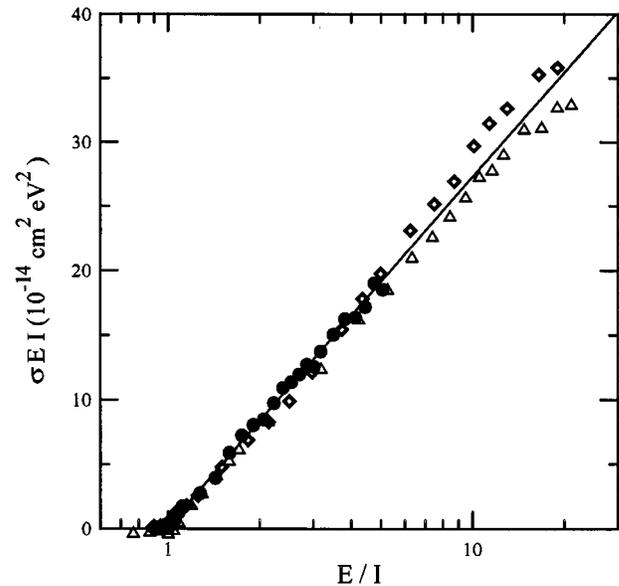

FIG. 7. Bethe plot of product of scaled electron impact ionization cross sections times reduced energy versus the logarithm of the reduced energy for C-like ions. The circles are the present results for Ne^{4+}, the diamonds are measurements for O^{2+} from Ref. 18. The lines are least-squares fits to the experimental points.

FIG. 9. Bethe plot of product of scaled electron impact ionization cross sections times reduced energy versus the logarithm of the reduced energy for B-like ions. The circles are the present results for Ne^{5+}, the diamonds are measurements for O^{3+} from Ref. [20], and the triangles are measurements for N^{2+} from Ref. [19]. For clarity only the least-squares fit line for the Ne^{5+} data is shown.
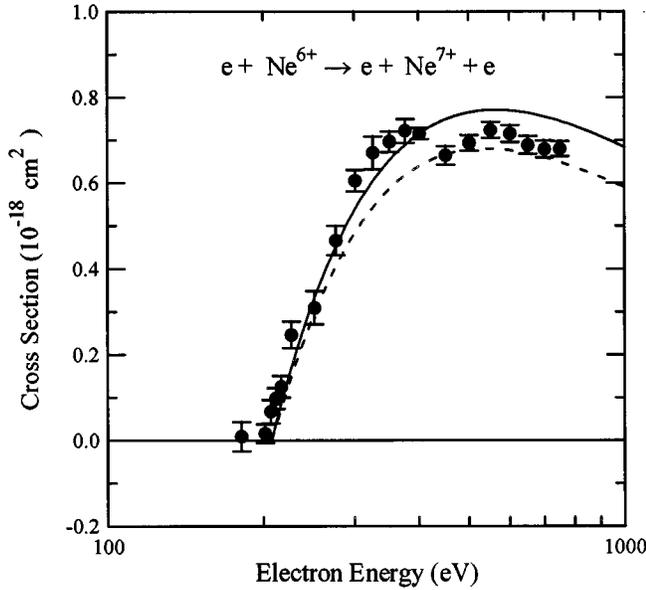
FIG. 10. Absolute cross sections as a function of electron-impact energy for single ionization of Ne^{6+}. The present experimental results are indicated by the solid circles with relative uncertainties at the one-standard-deviation level. The solid curve is the prediction of the one-parameter Lotz formula and the dashed curve represents the cross sections recommended in Ref. [8].
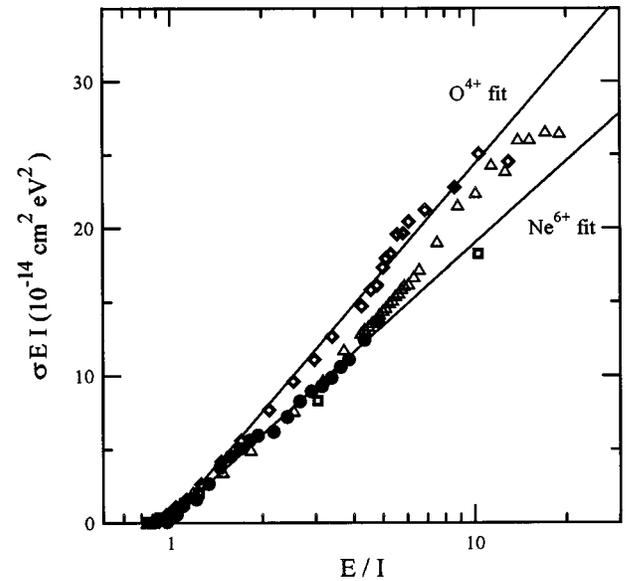
FIG. 11. Bethe plot of product of scaled electron impact ionization cross sections times reduced energy versus the logarithm of the reduced energy for Be-like ions. The circles are the present results for Ne^{6+}. The other measurements are from Ref. [22]: diamonds, O^{4+}, triangles, N^{3+}, and squares, C^{2+}. For clarity only the least-squares fit lines for the Ne^{5+} and O^{4+} data are shown.

ion gauge (PIG) ion source [22]. Further data are needed to determine whether this difference in metastable fractions is due to the sources used or to the details of atomic structure and population dynamics for the different species.

D. Ne^{6+}

Table V lists the measured cross sections for Ne^{6+} from 180 eV to 800 eV with relative uncertainties at the one-standard-deviation level and total uncertainties given in parentheses at a level equivalent to 90% confidence for the statistical uncertainties. The total uncertainty is typically 13% near the peak of the cross section. The present data are also shown in Fig. 10 with a solid curve representing the Lotz formula for direct ionization of the $2s^2$ ground state and a dashed line representing the recommendation of Lennon *et al.* [8] based on the distorted-wave calculations of Jakubowicz and Moores [15] for Ne^{6+}.

Unlike the measurements for the other three neon ions, the experimental results for Ne^{6+} agree better with the recommended curve than the Lotz formula for energies above 400 eV. Below 400 eV, the Lotz prediction is closer. No metastables were found in the ion beam, as evidenced by the zero cross sections below the 207.27 eV ground state threshold [17].

A comparison of the present measurements with those for ionization of other isoelectronic ions [23] is shown in the Bethe plot of Fig. 11. The scaled cross sections for Ne^{6+} are in very good agreement with those for C^{2+} and N^{3+}, but 10–15% lower than the scaled cross sections for O^{4+}. It should be noted, however, it was estimated that about 90% of the ions in the C^{2+}, N^{3+}, and O^{4+} experiments were in metastable states when extracted from the ORNL PIG

source. As remarked previously, it is not clear whether the difference in metastable fractions between the present results and the older ones is due to using different types of ion sources or due to atomic physics of the different ions. One might expect that since the ECR ion source has a higher average electron temperature it would produce more metastables, but the trend shown here is just the opposite.

IV. RATE COEFFICIENTS

For many applications such as plasma modeling, it is useful to report Maxwellian rate coefficients for the process investigated. Table VI lists rate coefficients calculated from our present cross section measurements using a method described elsewhere [24] with the measured data extrapolated to high energies using ($\ln E/E$). In addition, the rate coefficients were fit with Chebyshev polynomials of the first kind, $T_n(x)$, to enable the user to calculate them for any temperature in the range 10^5 K $\leq T \leq 10^8$ K:

$$\alpha(T) = T^{1/2} e^{-I/kT} \sum_{j=0}^{n} a_j T_j(x), \qquad (3)$$

where I is the ionization potential. The coefficients $a_0, \ldots, a_8$ given in Table VII reproduce the rate coefficients to within 1% over the given temperature range. The rate coefficient $\alpha(T)$ can be expressed simply as

$$\alpha(T) = \tfrac{1}{2} T^{1/2} e^{-I/kT}(b_0 - b_2) \qquad (4)$$

with the coefficients b_0 and b_2 calculated using Clenshaw's algorithm [25]:

$$b_j = 2x b_{j+1} - b_{j+2} + a_j \quad j = 0, 1, 2, \ldots, 8, \qquad (5)$$

TABLE VI. Maxwellian rate coefficients (in units of cm^3/s) for the ionization of Ne^{q+} ($q=2,4$–6) at selected values of T (in K) calculated from the measured cross sections (see text).

Electron temperature	Ionization rate coefficients α (cm^3/s)			
T (K)	Ne^{2+}	Ne^{4+}	Ne^{5+}	Ne^{6+}
1.0×10^5	4.54×10^{-12}	1.36×10^{-15}	1.32×10^{-17}	3.60×10^{-20}
2.0×10^5	2.32×10^{-10}	2.19×10^{-12}	1.49×10^{-13}	4.76×10^{-15}
4.0×10^5	1.90×10^{-9}	9.84×10^{-11}	1.74×10^{-11}	2.07×10^{-12}
6.0×10^5	4.03×10^{-9}	3.64×10^{-10}	8.99×10^{-11}	1.67×10^{-11}
8.0×10^5	5.99×10^{-9}	7.11×10^{-10}	2.08×10^{-10}	4.86×10^{-11}
1.0×10^6	7.68×10^{-9}	1.07×10^{-9}	3.48×10^{-10}	9.26×10^{-11}
2.0×10^6	1.29×10^{-8}	2.49×10^{-9}	9.89×10^{-10}	3.43×10^{-10}
4.0×10^6	1.65×10^{-8}	3.73×10^{-9}	1.66×10^{-9}	6.65×10^{-10}
6.0×10^6	1.76×10^{-8}	4.15×10^{-9}	1.94×10^{-9}	8.26×10^{-10}
8.0×10^6	1.78×10^{-8}	4.30×10^{-9}	2.08×10^{-9}	9.14×10^{-10}
1.0×10^7	1.78×10^{-8}	4.34×10^{-9}	2.14×10^{-9}	9.65×10^{-10}
2.0×10^7	1.67×10^{-8}	4.16×10^{-9}	2.18×10^{-9}	1.04×10^{-9}
4.0×10^7	1.48×10^{-8}	3.70×10^{-9}	2.03×10^{-9}	1.01×10^{-9}
6.0×10^7	1.35×10^{-8}	3.38×10^{-9}	1.90×10^{-9}	9.59×10^{-10}
8.0×10^7	1.25×10^{-8}	3.15×10^{-9}	1.79×10^{-9}	9.15×10^{-10}
1.0×10^8	1.18×10^{-8}	2.97×10^{-9}	1.71×10^{-9}	8.77×10^{-10}

where $b_9=b_{10}=0$ and the reduced energy x is given by

$$x = \frac{\log_{10}T - 6.5}{1.5}. \tag{6}$$

The present results agree very well with published rate measurements for Ne^{5+}. Datla and Roberts [26] reported a rate coefficient of 1.08×10^{-10} cm^3/s at 55 eV and Schmidt *et al.* [27] measured 2.9×10^{-10} cm^3/s at 80 eV. The present results are 1.10×10^{-10} cm^3/s and 2.97×10^{-10} cm^3/s at 55 eV and 80 eV, respectively. The agreement is not so good for the ionization of Ne^{6+}, however. At 55 eV, the present result is 2.16×10^{-11} cm^3/s with Datla and Roberts [26] reporting a value of 3.8×10^{-11} cm^3/s. At 100 eV, the present result is 1.33×10^{-10} cm^3/s versus 1.8×10^{-10} cm^3/s measured by Schmidt *et al.* [27]. This discrepancy may be due to

the absence of metastable Ne^{6+} ions in the present experiment and their presence in the direct rate coefficient measurements [26,27].

V. SUMMARY

Absolute total cross sections for electron-impact single ionization of Ne^{q+} ($q=2,4$–6) ions were measured using the ORNL crossed-beams apparatus, with typical total uncertainties ranging from 9% for Ne^{2+} to 13% for Ne^{6+}. Cross sections for all four ions are dominated by direct processes and in good agreement with the predictions of the Lotz semiempirical formula as well as the data recommended by the data compilation of Lennon *et al.* [8]. The Ne^{2+} results were also in good agreement with the measurements of Matsumoto *et al.* [3]. The measurements for the other three ions

TABLE VII. Rate-coefficient fitting parameters. All parameters are in units of 10^{-13} cm^3 $K^{-1/2}$ s^{-1}. Rate coefficients in the range 10^5 K $\leqslant T \leqslant 10^8$ K may be calculated using these parameters in a Chebyshev polynomial expansion, or through Clenshaw's algorithm (see text).

Fitting parameter	Ne^{2+}	Ne^{4+}	Ne^{5+}	Ne^{6+}
a_0	185.787	58.4460	24.5603	7.16433
a_1	-80.0547	-28.9373	-10.3413	-1.35526
a_2	-17.6862	-0.889595	-2.40887	-2.55532
a_3	20.2390	4.61315	2.77899	1.32380
a_4	-1.91632	-0.707830	-0.473245	0.115278
a_5	-2.00383	-0.402223	-0.119709	-0.324250
a_6	0.0786975	0.111143	-0.0267319	0.115607
a_7	0.356676	0.00189733	0.0719363	0.0265578
a_8	0.000000	0.000000	-0.0247852	-0.0324881

were close to those for other isoelectronic multicharged ions when compared on a Bethe plot. Only the Ne^{4+} results suggested the possible presence of a small fraction of metastables in the incident ion beam.

[1] R. A. Phaneuf, Phys. Scr. **T47**, 124 (1993).

[2] A. Danjo, A. Matsumoto, S. Ohtani, H. Suzuki, H. Tawara, K. Wakiya, and M. Yoshino, J. Phys. Soc. Jpn. **53**, 4091 (1984).

[3] A. Matsumoto, A. Danjo, S. Ohtani, H. Suzuki, H. Tawara, T. Takayanagi, K. Wakiya, I. Yamada, M. Yoshino, and T. Hirayama, J. Phys. Soc. Jpn. **59**, 902 (1990).

[4] D. C. Gregory, P. F. Dittner, and D. H. Crandall, Phys. Rev. A **27**, 724 (1983).

[5] P. Defrance, S. Chantrenne, S. Rachafi, D. S. Belic, J. Jureta, D. Gregory, and F. Brouillard, J. Phys. B **23**, 2333 (1990).

[6] D. E. Post, J. Nucl. Mater. **220-222**, 143 (1995).

[7] W. Lotz, Z. Phys. **206**, 205 (1967).

[8] M. A. Lennon, K. L. Bell, H. B. Gilbody, J. G. Hughes, A. E. Kingston, M. J. Murray, and F. J. Smith, J. Phys. Chem. Ref. Data **17**, 1285 (1988).

[9] D. C. Gregory, F. W. Meyer, A. Müller, and P. Defrance, Phys. Rev. A **34**, 3657 (1986).

[10] G. H. Dunn and B. Van Zyl, Phys. Rev. **154**, 40 (1967).

[11] See, for example, M. F. A. Harrison, J. Appl. Phys. **17**, 371 (1966).

[12] J. B. Hasted and G. L. Awad, J. Phys. B **5**, 1719 (1972).

[13] M. Hamdan, K. Birkinshaw, and J. B. Hasted, J. Phys. B **11**, 331 (1978).

[14] E. D. Donets and V. P. Oysyannikov, J. I. N. R. Dubna Report No. P7-10780 [translation: Oak Ridge National Laboratory Report No. ORNL-TR-4616, 1977] (unpublished).

[15] H. Jakubowicz and D. L. Moores, J. Phys. B **14**, 3733 (1981).

[16] A. Salop, Phys. Rev. A **14**, 2095 (1976).

[17] C. E. Moore, *Ionization Potentials and Ionization Limits Derived from the Analyses of Optical Spectra*, National Standard Reference Data Series No. NBS 34 (National Bureau of Standards, Washington, D.C., 1970).

[18] P. A. Zeijlmans van Emmichoven, M. E. Bannister, D. C. Gregory, C. C. Havener, R. A. Phaneuf, E. W. Bell, X. Q. Guo, J. S. Thompson, and M. Sataka, Phys. Rev. A **47**, 2888 (1993).

[19] R. A. Phaneuf, R. K. Janev, and M. S. Pindzola, Oak Ridge National Laboratory Report No. ORNL-6090, 1987 (unpublished).

[20] M. Pieksma, M. E. Bannister, W. Wu, and C. C. Havener (unpublished).

[21] D. H. Crandall, R. A. Phaneuf, and D. C. Gregory, ORNL/TM-7020, Oak Ridge National Laboratory, 1979 (unpublished).

[22] M. L. Mallory and D. H. Crandall, IEEE Trans. Nucl. Sci. **NS-23**, 1069 (1976).

[23] R. A. Falk, G. Stefani, R. Camilloni, G. H. Dunn, R. A. Phaneuf, D. C. Gregory, and D. H. Crandall, Phys. Rev. A **28**, 91 (1983).

[24] D. H. Crandall, G. H. Dunn, A. Gallagher, D. G. Hummer, C. V. Kunasz, D. Leep, and P. O. Taylor, Astrophys. J. **191**, 789 (1974).

[25] C. W. Clenshaw, Math. Tables Comput. **9**, 118 (1955).

[26] R. U. Datla and J. R. Roberts, Phys. Rev. A **28**, 2201 (1983).

[27] T. Schmidt, H.-J. Kunze, and V. P. Shevelko, Phys. Rev. A **39**, 2769 (1989).